Available online at www.sciencedirect.com
SCIENCE DIRECT®
Journal of Solid State Chemistry 174 (2003) 310–318
JOURNAL OF SOLID STATE CHEMISTRY
http://elsevier.com/locate/jssc

Structural and spectroscopic studies of $BiTa_{1-x}Nb_xO_4$

Choong-Young Lee,[a,b] Rene Macquart,[a] Qingdi Zhou,[a] and Brendan J. Kennedy[a,*]

[a] *Centre for Heavy Metal Research, The School of Chemistry, The University of Sydney, Sydney NSW 2006, Australia*
[b] *Department of Chemical and Environmental Technology, Inha Technical College, Inchon 402-752 South Korea*

Received 3 December 2002; received in revised form 9 April 2003; accepted 22 April 2003

Abstract

Polycrystalline samples of type $BiTa_{1-x}Nb_xO_4$ ($0 \leqslant x \leqslant 1$) in both the orthorhombic and triclinic phases have been characterized by a combination of powder X-ray diffraction, UV-Vis and Raman spectroscopy. The addition of Nb to $BiTaO_4$ subtly alters the structure and spectroscopic properties of both the orthorhombic and triclinic oxides. The difference in bonding from the Nb 4*d* and Ta 5*d* electrons results in an unusual variation in the cell parameters in the orthorhombic form. In both structural types the addition of Nb results in a shift of the strong UV-Vis absorption feature towards the visible region. This feature noticeably broadens and shifts towards lower energy in the triclinic structures.

1. Introduction

Bismuth oxides are of considerable interest for a variety of reasons including their unusual electronic properties, as seen in the Bi containing high temperature superconductors [1], their catalytic properties, as illustrated by the bismuth-molybdate oxidation catalysts [2], in addition to being used as a paint pigment and dye in the cosmetics industry [3]. The rich array of important properties displayed by bismuth-containing oxides is coupled with the exceptionally low toxicity of Bi [4]. The latter is all the more remarkable given Bi^{3+} is isoelectronic with the toxic heavy metals Pb^{2+} and Tl^{+}. The replacement of Pb by Bi has significant environmental benefits and efforts to this end are taking place.

The intense color displayed by many bismuth-containing oxides including, for example, bismuth vanadate $BiVO_4$, coupled with the redox properties of Bi [5] has prompted a number of investigations of the activity of Bi oxides for use as a photocatalyst [6]. Photocatalysis has been proposed as a means of eliminating organic pollutants from the environment. To be successful in such environmental applications the photocatalyst needs to be both stimulated by relatively low-energy light and non-toxic. There is also growing interest in the use of niobium oxides either as a catalyst support or as the active catalyst itself. In the current context we note that the layered niobate $Sr_2Nb_2O_7$ has been shown to be an active photocatalyst [7] as has the layered Ta oxide $In_{1-x}Ni_xTaO_4$ [8].

The solid solutions $BiTa_{1-x}Nb_xO_4$ have been found to evolve H_2 by the photocatalytic decomposition of water [9]. Given the similarity in the chemical properties of Ta and Nb (and to a lesser extent V) solid solutions of these may be expected to provide a means to fine-tune the catalytic properties of these bismuth oxides, provided the structures of the ternary oxides show a progressive evolution from that of the end-members. $BiNbO_4$ is a member of the family of oxides of the type $BiMO_4$ $M = V$, Nb, Ta, Sb [10–13], and numerous structural studies of these oxides have been reported. $BiVO_4$ has been found to undergo an irreversible orthorhombic–-monoclinic transition, and the monoclinic form undergoes a second reversible transition to a tetragonal structure [12]. Both $BiNbO_4$ and $BiTaO_4$ undergo an irreversible orthorhombic–triclinic transition [10,11]. A key feature of these structures is the distorted environment of the Bi atoms as a consequence of the sterochemical activity of the Bi 6*s* electrons [13].

In their earlier work on $BiTa_{1-x}Nb_xO_4$ Zou et al. [9] described the optical spectra of five representative compositions, three in the orthorhombic form and two in the triclinic structure. Whilst they observed dramatic differences in the spectroscopy of the two structural types, the band gap in the triclinic compounds is

*Corresponding author. Fax: +61-2-9351-3329.
E-mail address: b.kennedy@chem.usyd.edu.au (B.J. Kennedy).

0022-4596/03/$ - see front matter
doi:10.1016/S0022-4596(03)00225-1

noticeably wider than that of the orthorhombic compounds, it was not possible to conclude from their work if replacement of Ta by Nb significantly altered either the structural or spectroscopic properties of these ternary oxides. Hence, it was not established if the properties of these types of oxides can indeed be tuned by suitable substitutions.

The objective of this work was to prepare single-phase samples of the type $BiTa_{1-x}Nb_xO_4$ in both the orthorhombic and triclinic forms and to establish the relationship between the structure and observed UV-Vis spectra. In this paper we describe the synthesis, structure and spectroscopic properties of these oxides.

2. Experimental

2.1. Synthesis

The polycrystalline samples of $BiTa_{1-x}Nb_xO_4$ ($x = 0$, 0.1, 0.2, 0.3…0.9, 1.0) were prepared by the solid state reaction of high purity Bi_2O_3, Ta_2O_5 and Nb_2O_5. The appropriate stoichiometric amounts of the precursors were finely ground for several minutes using an agate mortar and pestle and pressed into alumina crucibles. During the grinding a small amount of acetone was added in order to mix the materials homogeneously. The samples were preheated in air at 700°C for 48 h, in order to prevent melting of Bi_2O_3, and were then heated at successively higher temperatures in air with several intermediate grindings. The final firing temperatures and times required to prepare the orthorhombic and triclinic phases are given in Table 1.

2.2. X-ray powder diffraction

All samples were characterized by X-ray powder diffraction using a Shimadzu S6000 Diffractometer and Cu$K\alpha$ radiation (40 kV, 30 mA). Diffraction patterns were recorded over the 2θ range 10–90°, with a step size of 0.02° and a counting time of 10–15 s per step was used. During the measurements the divergence and antiscatter slits were 1° and the receiving slit was 0.3 mm.

2.3. Structural refinements

The structural refinements were performed using the Rietveld method with the PC version of the program Rietica [14]. The background was defined by a fourth-order polynomial in 2θ and was refined simultaneously with the profile parameters. A pseudo-Voigt function was chosen to generate the profiles. The Gaussian component has widths given by the function $(\mathrm{FWHM})^2 = U\tan^2\theta + V\tan\theta + W$ where U, V and W are refineable parameters.

2.4. Spectroscopic measurements

UV-Vis spectra were recorded using a KBr matrix on a Varian Cary-5 UV-Vis-NIR spectrophotometer. The solid state Raman spectra were recorded over the range 0–3600 cm^{-1} using a Bruker RFS100 FT-Raman spectrometer, which employed a Nd:YAG laser emitting at 1064 nm as the excitation source. Solid samples were prepared by grinding the powdered solid and pressing it into an aluminum disc. Raman spectra were collected at resolution of 4 cm^{-1} by the co-addition of 16 continuous scans using a laser power of 130 mW.

3. Results and discussion

3.1. Synthesis

The preparation of single-phase samples of the orthorhombic $BiTa_{1-x}Nb_xO_4$ oxides required careful

Table 1
Synthesis conditions and refined lattice parameters for the series $BiTa_{1-x}Nb_xO_4$. The orthorhombic phase was obtained by heating at the lower temperature (LT) and the triclinic phase at the higher temperature (HT)

x	Temp. LT (°C)	Time (h)	Temp. HT (°C)	Orthorhombic			Triclinic					
				a (Å)	b (Å)	c (Å)	a (Å)	b (Å)	c (Å)	α (°)	β (°)	γ (°)
0	900	48	1200	5.6384(2)	11.7730(4)	4.9608(2)	7.6647(2)	5.5884(2)	7.7878(2)	90.06(1)	77.04(1)	86.47(1)
0.1	950	48	1200	5.6416(1)	11.7722(2)	4.9631(1)	7.6607(2)	5.5846(1)	7.7967(2)	90.06(1)	77.10(1)	86.54(1)
0.2	925	24	1200	5.6440(3)	11.7613(7)	4.9638(3)	7.6569(3)	5.5808(2)	7.8120(3)	90.05(1)	77.17(1)	86.63(1)
0.3	925	72	1200	5.6470(2)	11.7605(4)	4.9658(2)	7.6524(3)	5.5760(2)	7.8184(3)	90.09(1)	77.19(1)	86.71(1)
0.4	925	48	1200	5.6542(3)	11.7562(6)	4.9693(3)	7.6498(6)	5.5722(5)	7.8311(6)	90.08(1)	77.26(1)	86.76(1)
0.5	925	48	1200	5.6595(4)	11.7477(7)	4.9717(3)	7.6418(5)	5.5628(4)	7.8464(5)	90.08(1)	77.28(1)	86.86(1)
0.6	950	120	1200	5.6666(4)	11.7411(9)	4.9762(4)	7.6384(6)	5.5616(5)	7.8646(6)	90.12(1)	77.32(1)	86.91(1)
0.7	950	120	1200	5.6749(4)	11.7376(7)	4.9807(3)	7.6322(5)	5.5561(4)	7.8854(5)	90.15(1)	77.41(1)	87.02(1)
0.8	975	24	1200	5.6831(3)	11.7298(5)	4.9857(2)	7.6305(5)	5.5485(4)	7.9142(5)	90.16(1)	77.45(1)	87.11(1)
0.9	975	48	1200	5.6836(2)	11.7240(4)	4.9862(2)	7.6210(8)	5.5437(7)	7.9280(8)	90.14(1)	77.47(1)	87.18(1)
1.0	975	48	1200	5.6827(2)	11.7170(4)	4.9854(2)	7.6226(8)	5.5426(7)	7.9357(8)	90.13(1)	77.49(1)	87.19(1)

monitoring of the temperatures used to prepare the oxides. Aurivillius described $BiNbO_4$ and $BiTaO_4$ as being isostructural [11]; with the niobate transforming irreversibly to the triclinic structure when heated above 1020°C whilst the transformation of $BiTaO_4$ to the triclinic structure occurs near 1150°C. Previous reports suggest the orthorhombic end-member oxides can be formed at 900–950°C [15,16]. There is a very small temperature range in which the orthorhombic phases can be prepared. We have found that when temperatures below those listed in Table 1 were employed in an attempt to prepare the target oxides the products were either poorly crystalline or contained appreciable amounts of impurity phases. At low Nb contents temperatures around 900–950°C yielded highly crystalline single-phase orthorhombic samples, somewhat higher temperatures being required to prepare the single-phase Nb rich samples. In order to avoid the formation of the triclinic phase it was found that prolonged heating at the tabulated temperatures was required to obtain the desired compound. Even small increases in temperature over that stated resulted in the formation of variable amounts of the triclinic phase. The preparation of the analogous triclinic phases was straightforward, in all cases these were obtained by heating the analogous orthorhombic phase at 1200°C for 24 h. The diffraction patterns of the Nb rich compounds showed the presence of a number of peaks that could not be indexed to either the triclinic or orthorhombic cells. It was not possible to identify this phase. No attempt was made to establish the composition dependence of the orthorhombic to triclinic transition temperature.

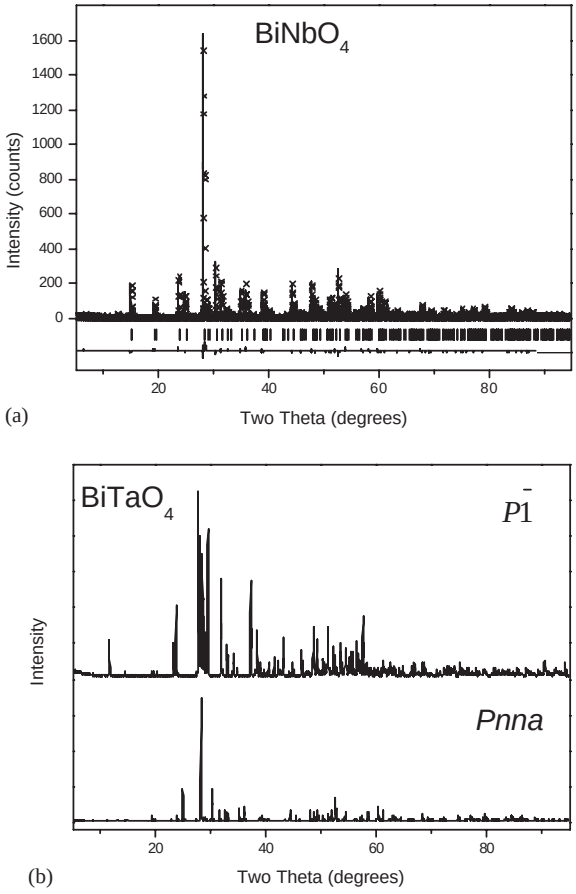

Fig. 1. (a) Observed, calculated and difference powder X-ray diffraction profiles for the orthorhombic structure of $BiNbO_4$. The short vertical markers show the positions of all the allowed Bragg reflections in space group *Pnna*. (b) Observed powder X-ray diffraction profiles for the orthorhombic and triclinic structure of $BiTaO_4$.

3.2. Orthorhombic samples

The sample purities were monitored using powder X-ray diffraction. All the diffraction peaks were indexed to an orthorhombic *Pnna* cell, and in all cases the Rietveld structural refinements yielded satisfactory agreements between the observed and calculated profiles, an example being shown in Fig 1. The orthorhombic structure of the $BiTa_{1-x}Nb_xO_4$ oxides is represented in Fig. 2. The refined structural and lattice parameters for the two end-member oxides $BiNbO_4$ and $BiTaO_4$ are given in Tables 1 and 2 and are in good agreement with values reported previously [9,15,17]. The orthorhombic structure can be viewed as a pseudo-layered structure in which layers of corner sharing NbO_6 octahedra are separated along the *b*-axis by Bi atoms. Six oxygen atoms in a distorted octahedral geometry surround the Bi atoms, with two of the Bi–O distances being very much longer than the other four (ca. 2.7 Å, cf. 2.2 Å), Table 3. A feature of the structure is the alternation of the Bi–Bi separation within the rows of Bi atoms, running along the c-axis; there being a short, 3.57 Å, and long, 3.96 Å, distance. An alternate description of the Bi coordination is with the Bi occupying the vertex of a BiO_4 square pyramid. Presumably the Bi $6s^2$ lone pair electrons occupy the "fifth" coordination site of the Bi atoms in this description. These 6*s* electrons apparently occupy the area between two adjacent Bi atoms, repelling both the oxygen and nearby Bi atoms, hence the alternating Bi–Bi separation.

The lattice parameters for the orthorhombic $BiTa_{1-x}Nb_xO_4$ compounds show strongly anisotropic behavior, Fig. 3. As the Nb content is increased the *a* and *c* parameters are increased whereas the *b*-parameter decreases. This results in the unusual variation in the cell volume illustrated in Fig. 3 where the volume is seen to initially increase as the Nb content increases to $x = 0.8$ before decreasing at still higher contents. The total volume change over the full composition range is very small, ca. 1%, and is in keeping with the similar size of Nb^V and Ta^V in an octahedral environment, both are reported to have ionic radii of 0.64 Å [18].

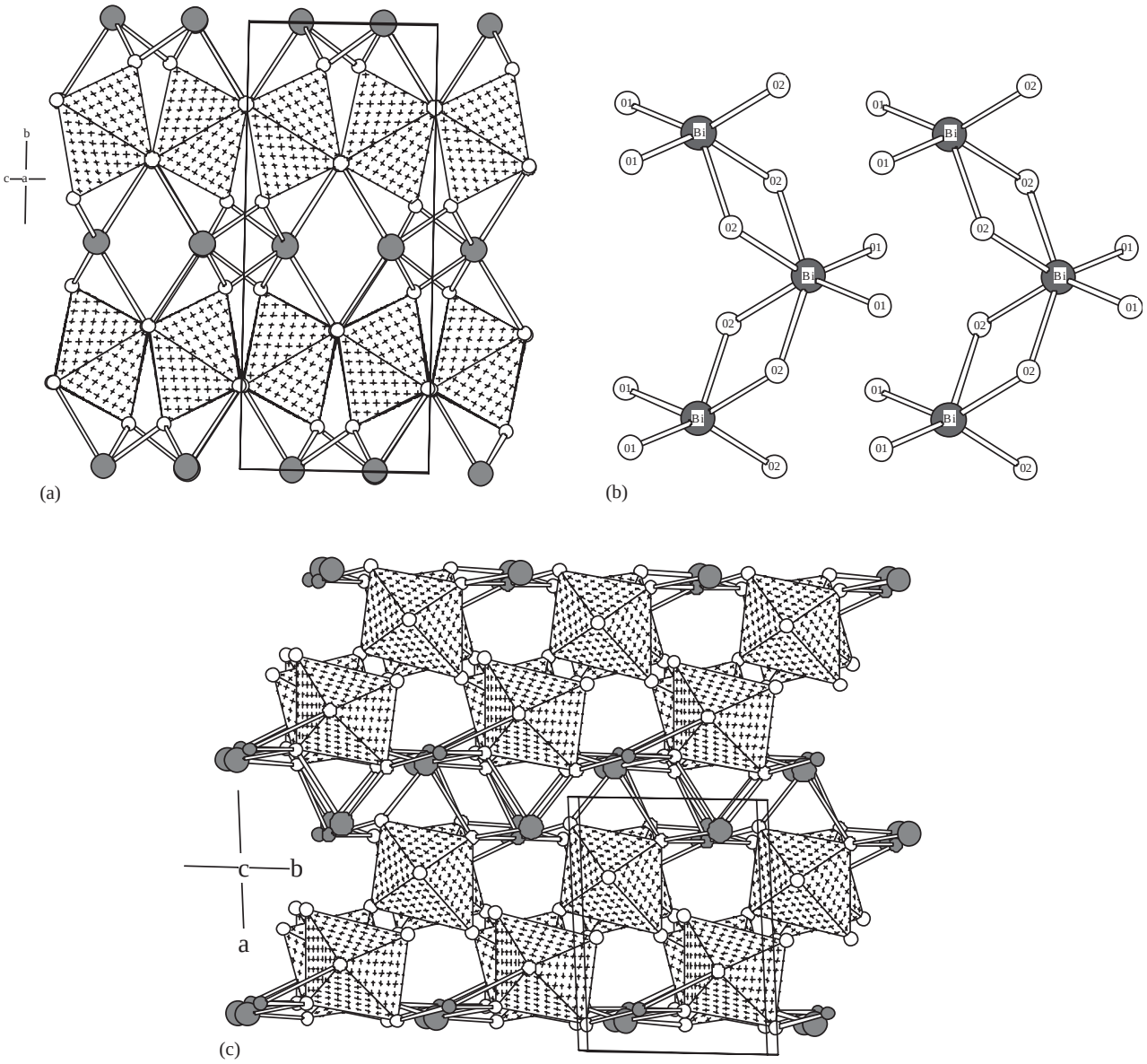

Fig. 2. (a) Representation of the orthorhombic $BiTaO_4$ structure. The corner sharing TaO_6 octahedra are represented by the shaded polyhedra, whilst the large shaded spheres represent the Bi atoms and the small spheres the oxygen atoms. The contents of the unit cell are indicated. (b) View of the local environment of the Bi atoms in orthorhombic $BiTaO_4$. The numbering of the oxygen atoms is the same as in Table 2. (c) Representation of the triclinic $BiTaO_4$ structure. The corner sharing TaO_6 octahedra are represented by the shaded polyhedra, whilst the large shaded spheres represent the Bi atoms and the small spheres the oxygen atoms. The contents of the unit cell are indicated.

Within the precision of the present structural refinements, which have used non-monochromatic Cu X-rays, the following conclusions on the structural variations across the $BiTa_{1-x}Nb_xO_4$ series can be made. (I) There is a small decrease in both the long and short Bi–Bi distance as the Nb content increases, (II) The short Bi–O distances do not significantly change across the series although there is a slight tendency for the long Bi–O distance to increase and (III) $M-O$ distances do not significantly change across the series, Table 3. The average $M-O$ distances are very close to the value estimated from the sum of the effective ionic radii (0.64 + 1.40 Å), however the six $M-O$ distances are not all equal indicating some variation in the bonding. Clearly more precise structural information as can be obtained using neutron or high-energy synchrotron powder diffraction would be beneficial to precisely quantify the subtle changes in the Bi–O and $M-O$ distances. Nevertheless, it is probable that there is some degree of covalency in the $M-O$ and Bi–O bonding.

The anisotropic variation in cell parameters is readily explained by examination of the structure. As the amount of, the apparently smaller, Ta present in the MO_6 octahedron increases there is a contraction within

the *ac* plane. This limits the amount of space available for the $6s^2$ lone pair of electrons within the Bi atom chains and these repel the adjacent MO_6 layers resulting in an expansion along the *b*-axis. Given the volume of the MO_6 octahedra does not significantly change across the series the contraction in the *ac* plane is presumably related to a change in the bonding. This change in bonding results in the Bi 6*s* electrons occupying a greater volume in the Nb rich compounds compared to the Ta rich compounds. This would also account for the small increase in the long Bi–O distance in the Nb rich oxides. In a study on $SrBi_2(Ta_{1-x}Nb_x)O_9$ Shimakawa and co-workers [19] concluded that the covalency of the $M-O$ bonds increased as the Nb content increased. This was postulated to be a consequence of the Nb 4*d* orbital being somewhat less extended than the Ta 5*d* orbitals, so that the hydridization of the Nb 4*d* and O 2*p* orbitals is favored resulting in a more covalent bond. If the same arguments are valid in the present case then the increased covalency of the $M-O$ bonds upon Nb substitution results in greater localization of the Bi $6s^2$ electrons as a lone pair.

Table 2
Refined structural parameters for $BiNbO_4$ and $BiTaO_4$ at 25°C, space group *Pnna*. R_p 11.1, R_{wp} 16.0, R_{Bragg} 9.0, $\chi^2 = 1.26$ for $BiNbO_4$ and R_p 9.4, R_{wp} 14.4, R_{Bragg} 5.9, $\chi^2 = 1.23$ for $BiTaO_4$

Atom	Site	*x*	*y*	*z*	*B* (Å^3)
Bi	4*c*	1/4	0	0.7186(3)	1.9(1)
				0.7208(4)	**1.8(1)**
Nb/Ta	4*d*	0.3498(6)	1/4	1/4	2.2(1)
		0.3629(4)			**1.4(1)**
O(1)	8*e*	0.145(3)	0.314(2)	0.505(3)	1.8(5)
		0.136(3)	**0.303(2)**	**0.537(3)**	**1.5(5)**
O(2)	8*e*	0.583(3)	0.903(1)	0.593(3)	0.8(4)
		0.581(3)	**0.907(2)**	**0.594(3)**	**0.6(4)**

In the table body the lower set of figures, in bold, are the values for

The UV-Vis spectra for the 11 orthorhombic samples studied are all very similar and are dominated by an intense peak near 300 nm, Fig. 4. The absence of any features in the visible region is consistent with the appearance of the samples, all of which are a cream color. In all cases a broad shoulder is apparent between 450 and 350 nm. This shoulder appears to be much weaker in pure $BiNbO_4$ and appears to be diagnostic of the presence of Ta in the samples. As evident from Fig. 4 the main peak near 300 nm is clearly not Gaussian in shape and presumably is the result of at least two processes. It is probable that this feature is a result of a Bi–O charge transfer process and consists of two transitions arising from the two markedly different Bi–O bond lengths seen in the structures, ca. 2.7 and 2.2 Å. The peak near 350 nm moves to progressively longer wavelength as the Nb content increases indicating a slight broadening of the band gap. Since it is most probable that this feature is due to a Bi–O transition this implies a change in the bonding of the Bi atoms. This is consistent with the structural and Raman studies that demonstrate a systematic shift from $BiTaO_4$ to $BiNbO_4$.

Whilst the Raman spectra of orthorhombic $BiTaO_4$ and $BiNbO_4$ appear substantially different, the spectra of the series of solid solutions demonstrates this to be a result of an evolution from one spectral extreme to the other, Fig. 5. For example, the splitting of the pair of peaks near 150 cm^{-1} in $BiTaO_4$ is absent in the spectra of $BiNbO_4$ as a result of a systematic reduction in the frequency of the higher energy peak. In the absence of a normal mode analysis of the complexes it is not possible to assign the observed peaks however a number of observations can be made. It is assumed that the bands below ca. 500 cm^{-1} are generated by first-order modes, whereas multiphonon or electronic Raman processes are the probable cause of the Raman peaks at higher wavenumbers. Firstly, it is possible to identify a number of peaks the frequencies of which are independent of the Nb:Ta ratio, such peaks, e.g., those at 64 and 540 cm^{-1}

Table 3
Refined bond distances for the low temperature orthorhombic compounds in the series $BiTa_{1-x}Nb_xO_4$

x	Bi–Bi (Å)	Bi–O1 (Å)	Bi–O2 (Å)	Bi–O2 (Å)	Ta–O1 (Å)	Ta–O1 (Å)	Ta–O2 (Å)
0	3.952(2)	2.69(2)	2.13(2)	2.25(2)	2.01(2)	1.97(2)	2.03(2)
0.1	3.956(2)	2.67(2)	2.11(2)	2.30(2)	1.94(2)	2.07(2)	2.02(2)
0.2	3.959(3)	2.77(2)	2.08(2)	2.27(2)	1.95(2)	2.00(2)	2.09(2)
0.3	3.958(3)	2.70(2)	2.16(2)	2.23(2)	1.80(2)	2.23(2)	2.02(2)
0.4	3.962(2)	2.76(2)	2.09(2)	2.27(2)	1.86(2)	2.12(2)	2.06(2)
0.5	3.968(3)	2.74(2)	2.16(2)	2.28(2)	1.93(2)	2.05(2)	2.00(2)
0.6	3.970(3)	2.79(2)	2.11(2)	2.24(2)	1.89(2)	2.07(2)	2.08(2)
0.7	3.983(2)	2.70(2)	2.24(2)	2.23(2)	1.88(2)	2.15(2)	1.97(2)
0.8	3.993(2)	2.67(2)	2.13(2)	2.31(2)	1.88(2)	2.18(2)	2.01(2)
0.9	3.983(3)	2.60(2)	2.17(2)	2.34(2)	1.93(2)	2.19(2)	1.95(2)
1.0	3.993(2)	2.65(2)	2.143(2)	2.29(2)	1.88(2)	2.02(2)	2.00(2)

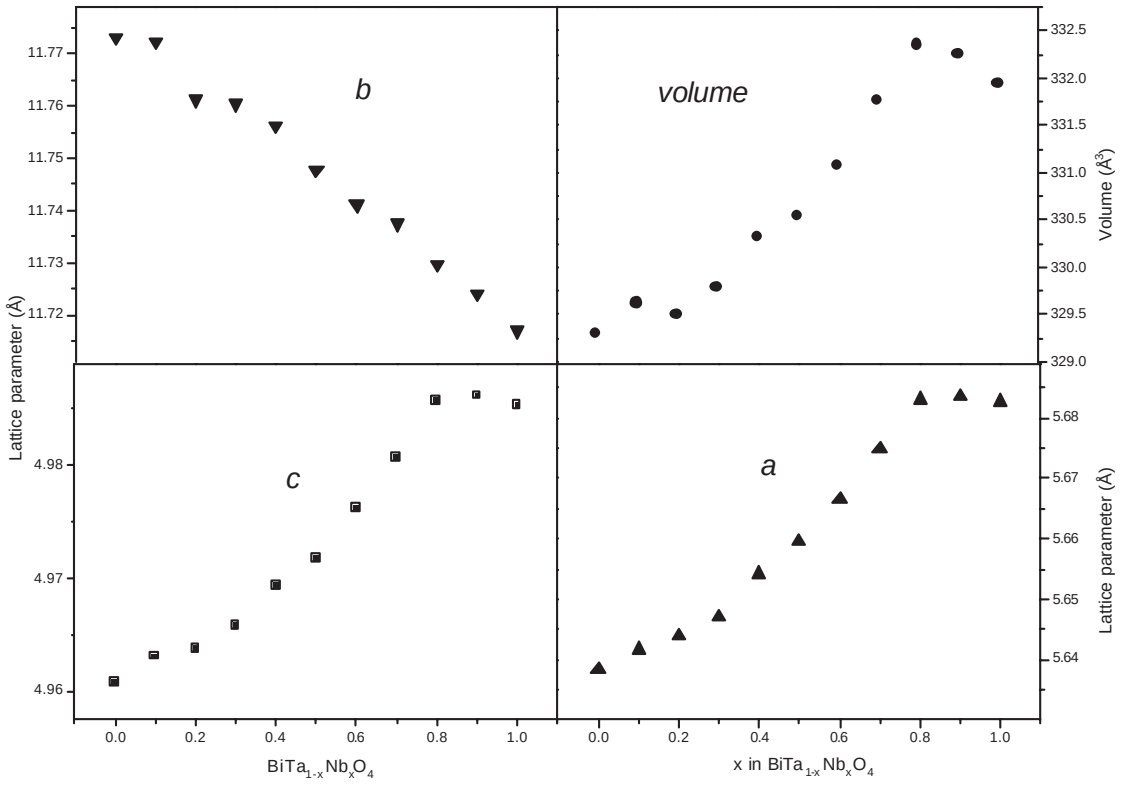

Fig. 3. Variation of the refined lattice parameters with composition for the orthorhombic structure observed in the series $BiTa_{1-x}Nb_xO_4$. In all cases the esds are smaller than the symbol.

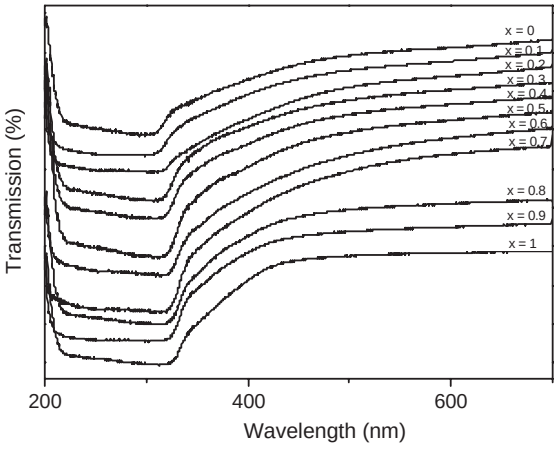

Fig. 4. UV-Vis spectra for the 11 orthorhombic samples in series $BiTa_{1-x}Nb_xO_4$. The composition varies from $x = 1$ at the bottom to $x = 0$ at the top in 0.1 steps. The traces have been vertically offset for the sake of clarity.

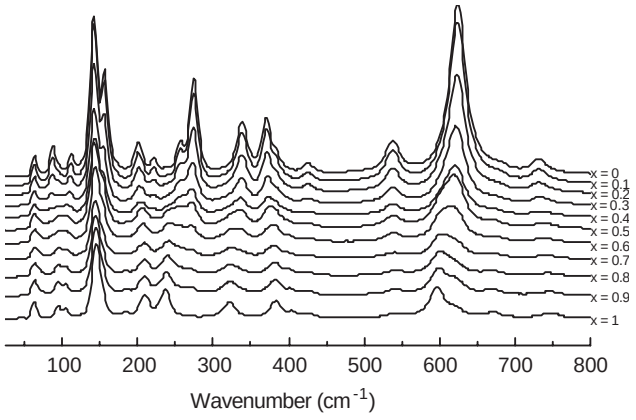

Fig. 5. Raman spectra for the 11 orthorhombic samples in series $BiTa_{1-x}Nb_xO_4$. The composition varies from $x = 1$ at the bottom to $x = 0$ at the top in 0.1 steps. The traces have been vertically offset for the sake of clarity.

are presumably Bi–O modes. Secondly, although a number of peaks move to lower frequencies as the Ta content increases, presumably reflecting the greater mass of the Ta atoms relative to the Nb atoms, others move to higher frequencies, Table 4. This is most apparent for the pair of peaks near 320/380 cm^{-1} in $BiTaO_4$. This is believed to reflect changes in the Nb/Ta–O–Nb/Ta angle altering the relative energies of the symmetric and antisymmetric modes.

A further striking feature of the Raman spectra is the apparent increase in the intensity of the various modes seen in the spectra of $BiTaO_4$. This is thought to reflect changes in the nature of the bonding the less "covalent" bonds in $BiTaO_4$ spectra having the more intense bands. Finally, there appears to be a broadening of the various peaks in the mixed Ta/Nb samples compared to those seen in pure $BiTaO_4$ or $BiNbO_4$. As indicated above the diffraction measurements have demonstrated that highly

Table 4
Selected Raman bands (cm^{-1}) for orthorhombic $BiTa_{1-x}Nb_xO_4$

$x=1$	$x=0.9$	$x=0.8$	$x=0.7$	$x=0.6$	$x=0.5$	$x=0.4$	$x=0.3$	$x=0.2$	$x=0.1$	$x=0$
64.1	64.1	64.1	64.1	64.1	64.1	64.1	64.1	64.1	64.1	64.1
94.9	94.9	96.9	96.9	96.9	96.9	87.2	87.2	87.2	87.2	87.2
104.6	104.6	104.6	104.6	106.5	106.5	108.4	110.4	110.4	112.3	112.3
145.1	145.1	145.1	145.1	145.1	143.1	143.1	143.1	143.1	143.1	143.1
					154.7	154.7	154.7	154.7	156.6	156.6
210.6	208.7	208.7	208.7	208.7	206.8	204.9	202.9	202.9	201.0	201.0
					220.3	220.3	222.2	222.2	222.2	222.2
237.6	239.6	241.5	241.5	243.4	243.4					
					256.9	256.9	256.9	256.9	256.9	256.9
270.4	270.4	270.4	270.4	272.4	272.4	272.4	272.4	274.3	274.3	274.3
322.5	322.5	324.4	324.4	334.1	336.0	337.9	337.9	337.9	339.8	339.9
384.2	384.2	382.3	382.3	380.4	376.5	374.6	372.6	372.6	372.6	370.7
544.3	542.3	542.3	542.3	540.4	540.4	540.4	540.4	538.5	538.5	538.5
598.3	600.2	602.1	604.0	617.55	621.4	621.4	623.3	625.3	625.3	625.3

crystalline single-phase samples have been obtained. However, whereas the diffraction measurements are sensitive to long-range ordering the Raman spectra are expected to be sensitive to short-range order and the observed broadening possibly reflects short-range ordering of the Nb and Ta atoms [20]. This would give rise to a range of Ta–O–*M* contacts and a range of frequencies of the associated modes. The need to prepare the solid solutions at relatively low temperatures may be a factor in promoting such short-range ordering. This broadening is most obvious at longer wavenumbers since higher wavenumber modes are characterized by shorter correlation lengths compared to low wavenumber modes [21].

3.3. Triclinic samples

The powder XRD pattern of $BiTaO_4$ heated to 1200°C could be indexed to a triclinic $P\bar{1}$ cell. The transition from the orthorhombic to triclinic phase is easily followed in the powder diffraction patterns, Fig. 1b. While a structure could be refined from the laboratory X-ray diffraction data using the Rietveld method the esds for the positional parameters of the light oxygen atoms were unacceptably high and some of the distances were unacceptable. The key features of the refined structure were consistent with those described by Keve and Skapski [16] for $BiNbO_4$ and contain two different Nb/Ta sites in the triclinic cell. The triclinic structure can also be viewed as a pseudo-layered structure in which the corner sharing Nb/TaO_6 octahedra are separated by layers of Bi atoms, Fig. 2. The Bi atoms are coordinated to eight oxygen atoms in a distorted square antiprism arrangement. High-resolution neutron diffraction data would be needed to obtain accurate structures of these low symmetry oxides.

Consequently, cell parameters were estimated using the Le Bail method as implemented in Rietica [14]. This enabled accurate lattice parameters to be obtained across the series $BiTa_{1-x}Nb_xO_4$ despite the presence of variable amounts of an unidentified impurity on the Nb rich compounds with $x>0.5$. The refined lattice parameters are given in Table 1. As found for the orthorhombic phase the volume of the triclinic cell was found to increase as the Nb content increased. Again the variation in cell parameters is anisotropic with the *a*- and *b*-axis decreasing as the Nb content increased whereas the *c*-axis increased.

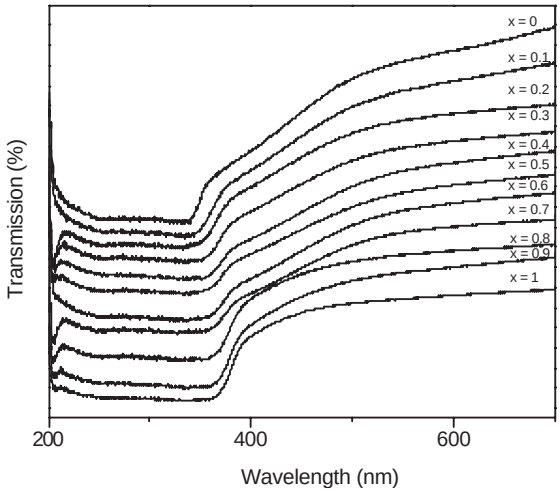

Fig. 6. UV-Vis spectra for the 11 triclinic samples in series $BiTa_{1-x}Nb_xO_4$. The composition varies from $x=1.0$ at the bottom to $x=0$ at the top in 0.1 steps. The traces have been vertically offset for the sake of clarity.

The UV-Vis spectra of the triclinic compounds, as illustrated in Fig. 6, show a progressive broadening of the strong feature near 350 nm as the Nb content increases. As for the orthorhombic compounds there is no evidence for any electronic transitions in the visible region and the compounds are all an off-white/cream color. Comparison of the UV-Vis spectra of any pair of triclinic–orthorhombic oxides shows the absorption feature in the triclinic phase commences at somewhat lower energy (higher wavelength). An identical effect

was observed in the earlier work of Zou et al. [9]. This suggests the triclinic oxides would be more suitable for use in photoelectric applications than the analogous orthorhombic compounds. Further, the progressive shift in the transition to higher wavelengths as the Nb content increases results in triclinic $BiNbO_4$ having absorption over the widest energy range into the visible region. Clearly doping with Nb tunes the band gap, and the progressive shift over the entire range of compositions shows that the addition of Nb systematically increases this.

The Raman spectra of the 11 triclinic oxides in the series $BiTa_{1-x}Nb_xO_4$ are all very similar with each other, Fig. 7, and noticeably more complex than that seen for the analogous orthorhombic oxides. The positions and intensities of the Raman peaks are expected to be sensitive to the local geometry of the Bi and Ta/Nb cations and the observed increase in the complexity of the spectra is a consequence of the increased number of modes that become Raman active as the symmetry is lowered. The spectra of $BiNbO_4$ shows the best resolved peaks, with various peaks broadening and weakening as the Ta content increases. As a technique Raman is sensitive to short-range order and the broadening of the various peaks is possibly indicative of some short-range disorder as the Ta content increases. The fact that this persists for pure $BiTaO_4$ is somewhat unexpected.

It is possible to distinguish between the triclinic and orthorhombic forms of $BiTa_{1-x}Nb_xO_4$ by Raman spectroscopy and this would be advantageous if the oxide were dispersed onto a high surface area support for use in photocatalytic applications. It is not apparent that Raman spectroscopy is a suitable method to monitor the incorporation of Nb into triclinic $BiTa_{1-x}Nb_xO_4$ solid solutions, although a number of peaks in the Raman spectra show progressive shifts as the Nb content increases indicating a systematic shift in the environment of the BiO_8 and Nb/TaO_6 groups, Table 5. This is best illustrated by the almost linear shift in the band near 400 cm^{-1} from 399 cm^{-1} in $BiTaO_4$ to 384 cm^{-1} in $BiNbO_4$, Fig. 8.

4. Conclusions

Powder samples of the Bi oxides $BiTa_{1-x}Nb_xO_4$ ($0 \leqslant x \leqslant 1$) in both the orthorhombic and triclininc phases have been characterized by a combination of

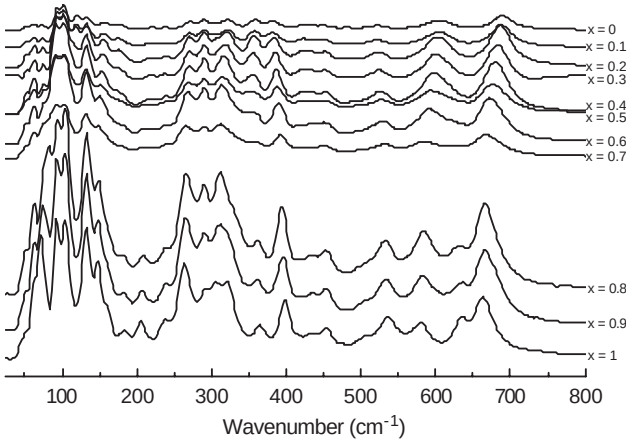

Fig. 7. Raman spectra for the 11 triclinic samples in series $BiTa_{1-x}Nb_xO_4$. The composition varies from $x = 1.0$ at the bottom to $x = 0$ at the top in 0.1 steps. The traces have been vertically offset for the sake of clarity.

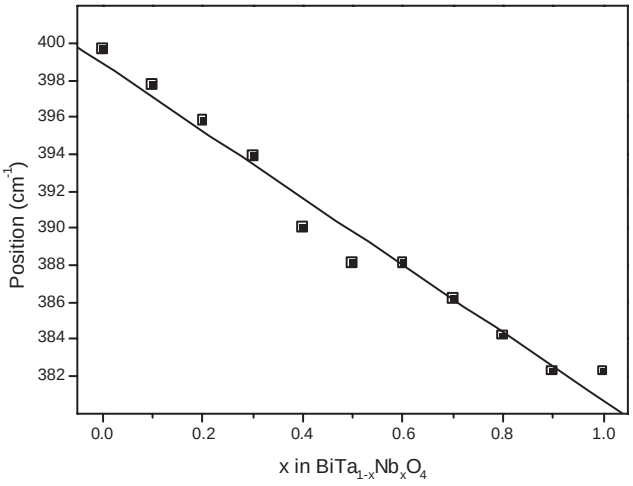

Fig. 8. Variation of the position of the Raman peak near 400 cm^{-1} in the triclinic oxides of the type $BiTa_{1-x}Nb_xO_4$. The solid line is a liner fit to the observed data.

Table 5
Selected Raman bands (cm^{-1}) for triclinic $BiTa_{1-x}Nb_xO_4$

$x = 1$	$x = 0.9$	$x = 0.8$	$x = 0.7$	$x = 0.6$	$x = 0.5$	$x = 0.4$	$x = 0.3$	$x = 0.2$	$x = 0.1$	$x = 0$
183.6	183.6	181.7								
364.9	361.1	363.0	359.1	355.3	355.3	355.3	357.2	357.2	359.1	359.1
399.6	397.7	395.8	393.8	390.0	388.1	388.1	386.1	384.2	382.3	382.3
536.6	534.6	532.7	532.7	530.8	526.9	526.9	525.0	523.1	523.1	521.1
580.9	582.8	584.8	584.8	590.5	594.4	598.3	600.2	604.0	606.0	607.9
636.8	636.8	632.9								
663.8	665.8	665.8	667.7	673.5	677.3	681.2	683.1	686.9	688.9	690.8

powder X-ray diffraction, UV-Vis and Raman spectroscopy. The addition of Nb to $BiTaO_4$ has very little effect on either the structure or spectroscopic properties of the orthorhombic oxides, although the difference in bonding between Ta and Nb results in an unusual anisotropic variation in the lattice parameters across the series of solid solutions. As found previously an irreversible structural transition to the triclinic structure occurs if the oxides are heated to above around 1000°C. The lower symmetry structures have more complex Raman spectra, but more interestingly the UV-Vis band has broadened considerably and shifted towards the visible region. As indicated in the introduction Bi oxides are of interest as photocatalysts. This requires a wide bad gap and in this regard the wider band gap of the triclinic oxides makes these a more attractive candidate for use in photocatalysis than the analogous orthorhombic oxides. The UV-Vis studies clearly show that the band gap is tuned by changing the Ta/Nb ratio, and in the orthorhombic complexes, at least, it appears that this is a consequence of the altered Bi–O bond distances.

Acknowledgments

The authors thank Dr. E. Carter for assistance in carrying out the Raman measurements. This work was partially supported by the Australian Research Council.

References

[1] C.N.R. Rao, J. Gopalakrishnan, New Directions in Solid State Chemistry, 2nd Edition, Cambridge University Press, Cambridge, 1997.
[2] D.J. Buttrey, T. Vogt, U. Wildgruber, W.R. Robinson, J. Solid State Chem. 111 (1994) 118.
[3] G. Buxbaum (Ed.), Industrial Inorganic Pigments, Wiley, VCH, 1998.
[4] N.C. Norman (Ed.), Chemistry of Arsenic, Antimony and Bismuth, Blackie Academic Professional, New York, 1998.
[5] J.-D. Grunwaldt, M.D. Wildberger, T. Mallat, A. Baiker, J. Catal. 177 (1998) 53.
[6] Z. Zou, J. Ye, H. Arakawa, Chem. Mater. 13 (2001) 1765.
[7] D.W. Hwang, H.G. Kim, J. Kim, K.Y. Cha, Y.G. Kim, J.S. Lee, J. Catal. 193 (2000) 40.
[8] Z. Zou, J. Ye, K. Sayama, H. Arakawa, Nature 414 (2001) 625.
[9] Z. Zou, J. Ye, H. Arakawa, Solid State Commun. 119 (2001) 471.
[10] R.S. Roth, J.L. Waring, Am. Mineralogist. 48 (1963) 1348.
[11] B. Aurivellius, Ark. Kemi 3 (1951) 153.
[12] A.K. Bhattacharya, K.K. Mallick, A. Hartridge, Mater. Lett. 30 (1997) 7.
[13] B.J. Kennedy, Powder Diffraction 9 (1994) 164.
[14] C.J. Howard, B.A. Hunter, A Computer Program for Rietveld Analysis of X-ray and Neutron Powder Diffraction Patterns, NSW, Australia, Lucas Heights Research Laboratories, 1998, pp. 1–27.
[15] E.T. Keve, A.C. Skapski, Chem. Commun. (1967) 281.
[16] E.T. Keve, A.C. Skapski, J. Solid State Chem. 8 (1973) 159.
[17] Y.S. Yu, H.C. Lee, H.K. Kim, S.G. Han, J.H. Lee, J.Y. Song, G.I. Lee, M.S. Jang, Ferroelectrics 107 (1990) 225.
[18] R.D. Shannon, Acta Crystallogr. A 32 (1976) 751.
[19] Y. Shimakawa, Y. Kubo, Y. Tauchi, T. Kamiyama, H. Asano, F. Izumi, Appl. Phys. Lett. 77 (2000) 2749.
[20] E. Hussin, L. Abellom, A. Morell, Mater. Res. Bull. 25 (1990) 539.
[21] I. Charrier-Cougoulic, T. Pagnier, G. Lucazeau, J. Solid State Chem. 142 (1999) 220.